The 9th European Congress on Computational Methods in Applied Sciences and Engineering
ECCOMAS Congress 2024
3–7 June 2024, Lisboa, Portugal

TOWARDS INDUSTRIAL RELEVANCE: UNCERTAINTY IN NUMERICAL RESISTANCE SPOT WELDING MODELS

B. Verkens[1,2], P. Van Rymenant[1], M. Faes [3] and D. Moens[1,2]

[1] KU Leuven, Department of Mechanical Engineering, LMSD division
Jan Pieter de Nayerlaan 5, 2860 Sint-Katelijne-Waver, Belgium
e-mail: {bouwe.verkens, patrick.vanrymenant, david.moens}@kuleuven.be

[2] Chair of Reliability Engineering, TU Dortmund
Leonhard-Euler-Strasse 5, 44227, Dortmund, Germany
email: matthias.faes@tu.dormund.de

Key words: Resistance spot welding, Finite element simulation, Uncertainty, Validation, Electro-thermomechnical model

Summary.

Numerical modelling of spot welding processes (RSW) provide valuable insights in the behaviour of the process. Previous studies examined phenomena such as the formation of the intermetallic compound layer in dissimilar welding, transport phenomena and the impact of the electrode geometry on the weld formation. These numerical models enhance the industry by predicting RSW quality in advance, enabling adjustments to welding schedules, where needed, to ensure optimal weld quality. However, the translation of current numerical model predictions to real-world welding scenarios faces some challenges by the uncertainties inherent to the process and input parameters.

This paper explores uncertainty in spot welding numerical models, aiming to augment current deterministic model predictions. To achieve this, the variation in input process parameters is propagated through a finite element model, and the distribution of the output—namely, the weld nugget diameter—is analyzed. By propagating uncertainties, the central moments characterizing the output distribution are derived, providing a more realistic representation of the real-world spot welding scenario. The numerical model employed is a 2D axisymmetric multiphysical finite element model, which offers temperature history and final nugget shape predictions using the software Simufact Forming 2023.4. To reduce computation time, the study proposes a method for simplifying measured current profiles while preserving energy input. This method is compared with the original measured current profiles, and the resulting nugget diameters are evaluated.

Validation involves comparing the weld nugget geometry obtained through simulation with actual measurements. The primary focus of this validation is to assess whether the finite element model is capable of approximating the real-life variation in weld diameter by propagating the variation in input process parameters, including the current profile and electrode force.

1 INTRODUCTION

Resistance spot welding (RSW) is a widely used joining process in various industries, particularly in automotive manufacturing, where it is employed to join thin overlapping metal sheets. The process is favored for its energy efficiency, economic viability, and suitability for automation, making it an essential technique in large-scale production environments [1].

The advancement of numerical modeling, particularly the finite element method (FEM), has provided a powerful tool for simulating and optimizing RSW processes. Previous studies have demonstrated that complex phenomena can be modeled using FEM, such as the formation of intermetallic compound layer in dissimilar welding [2], transport phenomena [3] and the impact of the electrode geometry on the weld formation[4]. These numerical models provide a detailed prediction of thermal and mechanical behavior. As such, they allow us to study the RSW quality in advance, enabling adjustments to welding schedules, where needed, to ensure optimal weld quality without relying solely on costly and time-consuming physical experiments. However, the practical application of these FEM models in industrial settings is often hindered by the uncertainty and variability inherent in the real-world welding process. Even with fixed process parameters, the results can vary significantly from one weld to another, highlighting the need for models that can accurately predict and account for these uncertainties.

This research aims to bridge the gap between the theoretical capabilities of FEM and their industrial application by focusing on the uncertainty in numerical resistance spot welding models. Specifically, the study seeks to develop and validate a finite element model that is capable of predicting the variance in the process output, namely the nugget diameter, which is an important indicator of weld quality. By incorporating real-world measured data into the model and performing sensitivity analyses, this research assess the effectiveness of these models in replicating the observed variability in weld outcomes.

2 METHODOLOGY

2.1 Finite Element Model

The modeling of the welding process is based on the actual in-house spot welding setup, described in section 2.3. For this, an electro-thermal-mechanically coupled finite element model is developed using Simufact Forming 2023.4. A 2D axisymmetric approach is used to simplify the geometry while maintaining the most important features of the welding process. The axis of symmetry aligns with both the axis of the welding electrodes and the center of the welding nugget, as illustrated in Figure 1.

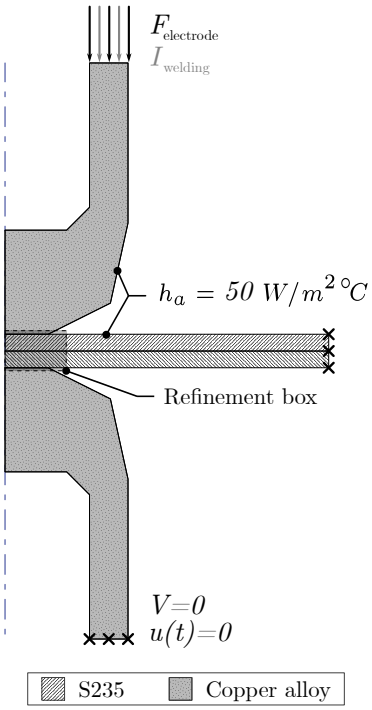

Figure 1: Schematic representation of the 2D axisymmetrical model

The geometry of the model consists of four different bodies from top to bottom : the upper electrode, the upper plate, the lower plate, and the lower electrode. The different analyses (i.e. electrical, thermal and mechanical) share the same geometry and mesh. The mesh of the finite element model consists of 6987 quadrilateral elements. A level-one refinement box is placed at the contact area between the base plates, refining the weld zone twice. The electrodes are modeled as rigid bodies to reduce computational complexity, focusing on interactions at the weld zone.

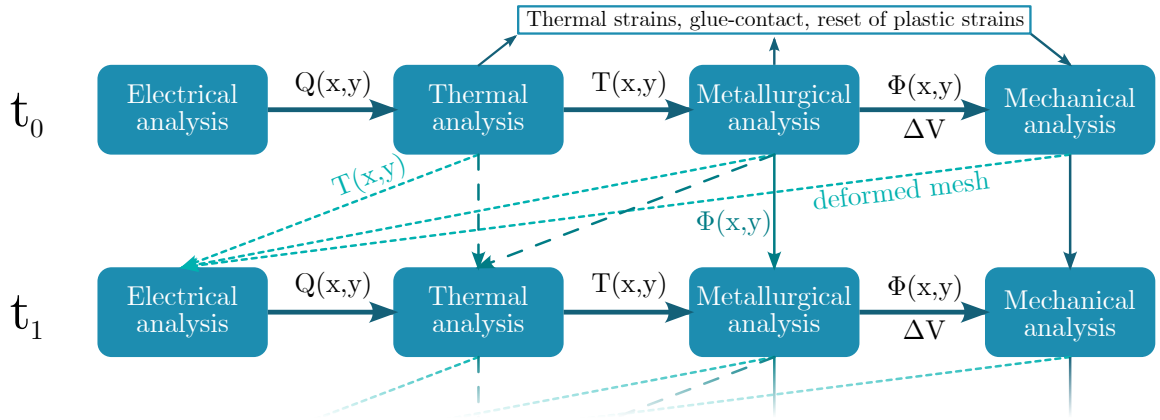

Figure 2: Schematic of the analyses coupling

The electro-thermo-mechanical model is weakly coupled, meaning that there is no feedback to previous analyses within a time-step. This is illustrated in figure 2. This coupling relies on small time steps to accurately account for real current scenarios, such as alternating current (AC) with a specific frequency [5].

Electrical analysis In this approach, an electrical analysis is performed to provide the thermal analysis with a current density, which in turn generates heat due to the Joule effect. First the electric field intensity vector $\vec{E}$ is described as:

$$\vec{E} = -\nabla V \tag{1}$$

where V denotes the electrical scalar potential. From this, the total current density vector can be obtained as follows:

$$\vec{J} = [\kappa]\,\vec{E}. \tag{2}$$

Here κ is the electrical conductivity matrix, written as:

$$[\kappa] = \begin{bmatrix} \frac{1}{\rho_{xx}} & 0 & 0 \\ 0 & \frac{1}{\rho_{yy}} & 0 \\ 0 & 0 & \frac{1}{\rho_{zz}} \end{bmatrix} \tag{3}$$

where ρ_{xx}, ρ_{yy} and ρ_{zz} are the electrical resistivity in x-, y- and z-directions. This electrical resistivity is temperature dependent and its value is of special importance at the contact interface of two bodies, in this case the plate material. At the start of the welding cycle, the electrical resistivity at these interfaces (electrode-plate and plate-plate) contribute significantly to the heat generation [1, 2]. The contact resistance ρ_c is modelled according to Bay-Wanheim [6, 7] as:

$$\rho_c = \frac{3\sigma_{soft}}{\sigma_n}\left(\frac{\rho_1 + \rho_2}{2} + \rho_{film}\right) \tag{4}$$

where σ_{soft} is the yield stress of the softest material, σ_n the normal stress, ρ_1 and ρ_2 are electrical resistivity of the materials in contact and ρ_{film} is the electrical resistivity of the film contimanent between the bodies. The layer thickness in this contact interface d_{film} is a modelling parameter.

The welding current $I_w(t)$ is applied to the upper electrode, as illustrated in figure 1, and a zero potential is applied to the lower electrode. Subsequently the Joule heat generation rate per unit volume yields:

$$Q(x, y) = \vec{J}^{\intercal}\vec{E} = \vec{E}^{\intercal}\,[\sigma]^{\intercal}\,\vec{E}. \tag{5}$$

Thermal analysis This heat generation $Q(x, y)$ is used as an imput to the thermal analysis to achieve the according thermal strains, contact changes and temperature profile. In this analysis, the governing PDE equals:

$$\nabla \cdot (q(x, y) + Q(x, y)) = \rho c \frac{dT}{dt} \tag{6}$$

with λ the thermal conductivity, T the temperature, ρ the mass density, c the specific heat constant and $q(x, y)$ the rate of heat flux and convection. The initial temperature of this analysis is set to 20°C and all external surfaces are modelled as convective with a convection

coefficient $h_a = 50\,\mathrm{W/m^2{}^\circ C}$. Finally, the contact type at the body interfaces is evaluated based on the temperature from this analysis. When the temperature at a node or segment reaches the liquidus temperature ($T_l = 1517°\mathrm{C}$) and subsequently cools down to the solidus temperature ($T_s = 1466°\mathrm{C}$), a glue contact is established. In this context, the gluing temperature is defined as the solidus temperature.

Mechanical analysis The temperature profile and contact conditions obtained from previous analysis directly influences the mechanical properties of the material involved. In this model, Young's modulus E, the flow curves, and thermal expansion coefficient α are temperature-dependent, while Poisson's ratio is kept constant. To account for the mechanical effects during the welding process, an electrode force $F_e(t)$ is applied to the upper electrode, while the bottom electrode is kept fixed in place. The governing equation the mechanical analysis solves is the equilibrium equation:

$$\nabla \cdot \vec{\sigma} + \vec{\mathbf{f}} = \rho \frac{d^2 \vec{\mathbf{u}}}{dt^2} \tag{7}$$

with σ representing the internal stresses within the material, $\vec{\mathbf{f}}$ the body force per unit volume, ρ the mass density and $\vec{\mathbf{u}}$ the displacement vector. Gravity is not taken into account and acceleration effects are generally neglected in spot welding, leaving f and $\frac{d^2\mathbf{u}}{dt^2}$ out of the equation, simplifying the equation to:

$$\nabla \cdot \vec{\sigma} = 0. \tag{8}$$

The relationship between the internal stress $\vec{\sigma}$ and the elastic strain $\vec{\epsilon}_{\text{elastic}}$ is given by:

$$\vec{\sigma} = \mathbf{C} : \vec{\epsilon}_{\text{elastic}}, \tag{9}$$

where $\mathbf{C}$ represents the fourth-order elastic stiffness tensor. The thermal expansion is accounted for by:

$$\vec{\epsilon}_{\text{thermal}} = \alpha(T - T_0), \tag{10}$$

where α is the thermal expansion coefficient, T is the current temperature, and T_0 is the reference temperature. Therefore, the total strain tensor $\vec{\epsilon}$ is expressed as:

$$\vec{\epsilon} = \vec{\epsilon}_{\text{elastic}} + \vec{\epsilon}_{\text{plastic}} + \vec{\epsilon}_{\text{thermal}}. \tag{11}$$

This formulation captures the combined effects of elastic, plastic, and thermal strains in the material under the given conditions.

2.2 FEM performance and sensitivity analysis

A sensitivity analysis was conducted to investigate which model parameters most affect the weld nugget diameter in the FEM of the resistance spot welding process. First, a surrogate model of the finite element model is constructed using a polynomial chaos expansion (PCE). This approach aids in efficiently approximating the complex behavior of the welding process and works as a computationally cost-effective substitute for the finite element model [8]. The inputs of interest in this model are four key process parameters—welding current profile (I_w), welding time ($\Delta t_{welding}$), rise time (Δt_{rise}), and electrode force ($F_{electrode}$)—as well as four model parameters—thickness of the contact layer (d_{XX}) and film resistance ($\rho_{film,XX}$) for both

plate-plate and electrode-plate contacts. The PCE is constructed by generating a Sobol sampling of 300 samples over the 8 input parameters of the finite element model. This stratified sampling method provides a more uniform and comprehensive exploration of the high-dimensional input space compared to traditional Monte Carlo sampling, leading to faster convergence and more accurate estimates with fewer samples. All input process and model parameters are modelled as

Table 1: Input process and model parameters

Input Parameter	**Nominal Value**	**Unit**	**Lower Limit**	**Upper Limit**
Welding current (I_w)	7.2	kA	3.5	10.5
Welding time ($\Delta t_{welding}$)	70	ms	0.035	0.105
Rise time (Δt_{rise})	10	ms	0.005	0.015
Electrode force ($F_{electrode}$)	2.5	kN	1.25	3.75
Thickness PP (d_{PP})	5×10^{-5}	m	2.5×10^{-5}	7.5×10^{-5}
Thickness EP (d_{EP})	5×10^{-6}	m	2.5×10^{-5}	7.5×10^{-5}
Film resistance PP ($\rho_{film,PP}$)	5×10^{-6}	$\Omega\cdot$ m	2.5×10^{-6}	7.5×10^{-6}
Film resistance EP ($\rho_{film,EP}$)	5×10^{-6}	$\Omega\cdot$ m	2.5×10^{-6}	7.5×10^{-6}

uniform distributions. Their nominal values, lower limit a and upper limit b can be found in Table 1.

The coefficients of the PCE model were calculated using the Least-Angule Regression (LARS) method. This approach selects the most significant basis functions from a large set of potential candidates, ensuring that the model remains both accurate and sparse. Additionally, a q-norm truncation of 1 is applied , retaining a moderate amount of polynomial terms, in order to avoid overfitting, yet capturing the complexity of the model. The resulting PCE converged at polynomial degree 4 and has a Leave-One-Out (LOO) cross-validation error of 6.9×10^{-2}.

Sobol indices Using the coefficients of the PCE surrogate model, Sobol indices are directly calculated to assess the sensitivity of the weld nugget diameter to the different input parameters. These indices reveal the contribution of each parameter to the variability in the weld nugget diameter, allowing for the identification of which inputs have the greatest influence. The Sobol indices are given by:

$$S_i = \frac{\text{Var}\left[\mathbb{E}[Y \mid X_i]\right]}{\text{Var}[Y]} \tag{12}$$

where S_i represents the sensitivity index for parameter i, $\mathbb{E}[Y \mid X_i]$ is the expected value of the output Y given parameter X_i, and $\text{Var}[Y]$ is the variance of the output [9, 10, 11].

Figure 3 shows the first-order and total Sobol indices. The first-order indices illustrate the individual contribution of each input parameter to the variation in the output. In this case, the welding current predominantly influences the variation in the resulting weld diameter. Higher welding currents typically produce larger nugget diameters, which is consistent with the increased heat generation leading to more extensive melting at the weld interface. In addition to the welding current, the welding time, electrode force, rise time and modelling parameters of the electrode-plate interface also contribute to the variation of weld diameter, but to a lesser extent.

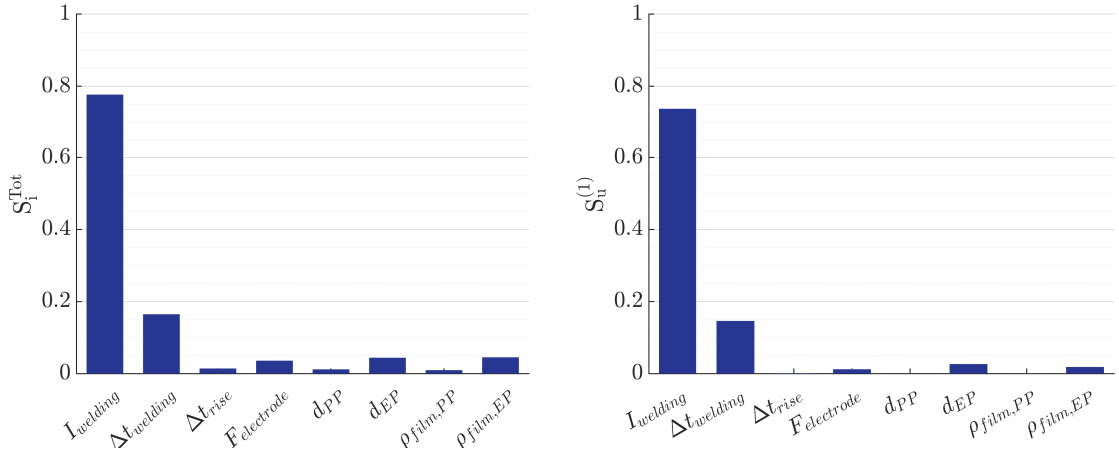

Figure 3: Total Sobol indices (left) and First Order Sobol indices (right)

Additionally, the Sobol indices indicate that the electric film resistance (ρ_{PP}) and thickness (d_{PP}) of the plate-plate interface do not directly contribute to the variation, as their first-order indices are equal to zero. However, their interaction with other input parameters does influence the variation in the output, as the total Sobol indices are non-zero.

SRC and SRRC sensitivity While Sobol indices are excellent for decomposing output variance, they don't offer insight whether the input parameters affects the output positively or negatively. To address this, a sensitivity analysis is conducted using standardized regression coefficients (SRC). This analysis is typically conducted within the context of multiple linear regression models. In such models, the output Y is assumed to be a linear combination of the input(s) X_i. Standardizing the regression coefficients b_i, which differ in scale, allows us to make meaningful comparisons. This standardisation helps to identify which input parameter(s) most significantly affects the model's output. The standardized regression coefficient for an input X_i is calculated as:

$$\beta_i = \frac{b_i \times \sigma_{X_i}}{\sigma_Y} \tag{13}$$

where β_i is the unstandardized regression coefficient, σ_{X_i} is the standard deviation of X_i, and σ_Y is the standard deviation of the dependent variable Y. By rescaling the coefficients, SRC sensitivity provides a clear, dimensionless measure of variable influence, aiding in the interpretation and prioritization of factors for further investigation or decision-making in model optimization [12].

While the SRC can provide insight in the direction of the effect of input parameters, it assumes a linear relationship. However, spot welding applications exhibit non-linear behaviour (weld formation). As an extension to the SRC, the standardized ranked regression coefficients (SRRC) are calculated as well. This involves replacing both the inputs X_i and the output Y with their respective ranks. After this rank transformation is performed, the SRC of this ranked data is calculated, as priory shown, leaving us with the standardized ranked regression coefficients. This method is particularly useful when the relationship between the input and output is monotonic but not linear, which is ideal in this case [11]. In Figure 4 the SRC and SRRC are plotted for each input parameter. From this, it is clear that the welding current $I_{welding}$, the welding

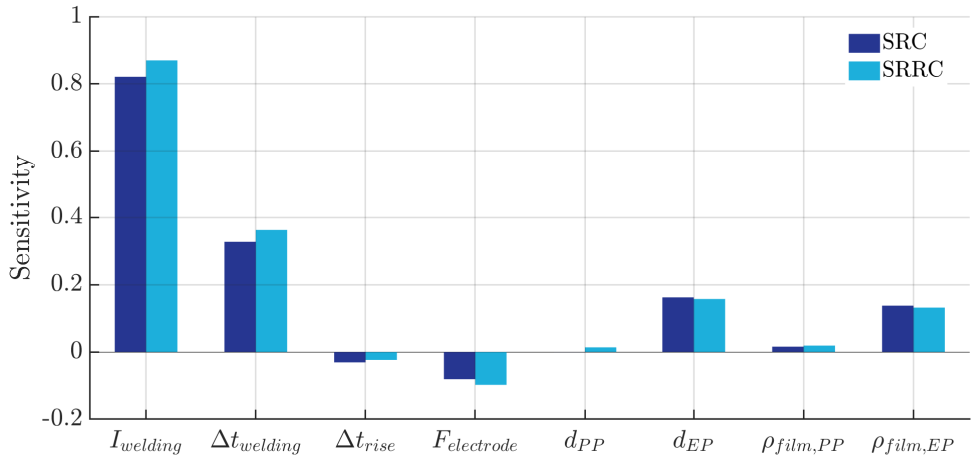

Figure 4: Standardized regression and rank regression coefficients

time $\Delta t_{welding}$ and the electrode force $F_{electrode}$ contribute the most to the formation of the nugget width, which is consistent with practical expectations of the process. The electrode force influences the diameter inversely proportional, which is to be expected. An increase in the electrode force raises the normal stress at the faying interfaces, which decreases the electrical contact resistance as can be seen in equation 4. This reduction in resistance results in lower Joule heat input and consequently a smaller final nugget. The larger differences between SRC and SRRC for some input parameters, particularly the welding current and time, underlines the non-linear relationship. The higher sensitivity in SRRC indicates that its effect on the output is better captured by a rank-based method, which are robust against non-linearities.

2.3 Materials and experimental design

The electrical current (I_w) was measured during spot welding of 50 samples of S235 steel plates with dimensions of 1 x 20 x 50 mm. Welding was executed using an ARO servo-actuated RSW machine of pedestal type with a medium frequency direct current (MFDC) power source (1000 Hz, 90 kVA). The welding parameters used in this study are listed in Table 2. The voltage (V_w) across the electrodes was measured during welding. All samples are welded with electrode caps with an ISO 8521 FE-15,8-5,5-30 geometry and are not replaced or cleaned in-between different samples.

Table 2: Overview of welding parameters

Process parameter	Value	Unit
Welding current (I_w)	7.2	kA
Welding time ($\Delta t_{welding}$)	70	ms
Electrode force ($F_{electrode}$)	2.5	kN

After welding, the samples are peeled and measured with a caliper according to ISO 10447:2006. The nugget diameter obtained from these measurements is denoted as d_{nugget}.

3 RESULTS AND DISCUSSION

3.1 Model simplifications

As mentioned in the introduction, the objective of this research is to utilize the actual current profile as input to the finite element model. However, this gives some computational challenges. The electric current is measured for over a 100 milliseconds at a sampling frequency of 2 MHz, resulting in a data array containing 200,000 data points. Performing a finite element analysis with 200,000 time steps would require an impractically long computing time, and selecting the number of time steps incorrectly could result in aliasing. Therefore, it is necessary to find a method to simplify this current profile accurately in order to reduce the computation time without significantly affecting the accuracy of the model.

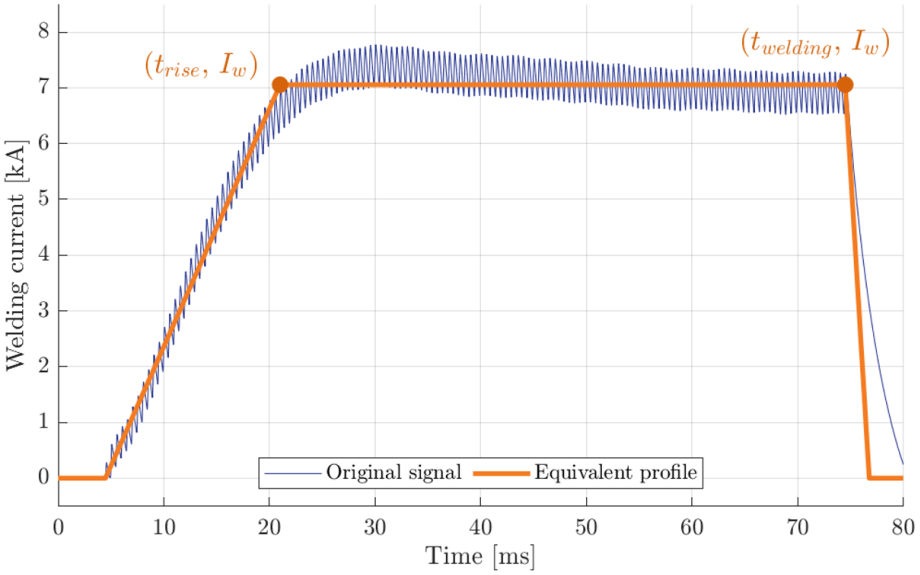

Figure 5: Measured and equivalent current profile

The method proposed in this research is based on conservation of the energy input into the weld. The goal is to identify an electrical current profile consisting of only 6 data points that delivers the same energy input as the measured original profile. To achieve this, the measured voltage and current are utilized, and determining the equivalent current profile involves solving an optimization problem. To begin with, the power at any instant in time t is given as the product of the measured voltage $V_w(t)$ and current $I_w(t)$:

$$P_w(t) = V_w(t) \cdot I_w(t). \tag{14}$$

The total energy input over the entire welding time is calculated as:

$$E_w = \int_{t_0}^{t_{end}} P_w(t)\, dt. \tag{15}$$

As the measured data is sampled at a certain sampling frequency f_{sampling} (2 MHz), the energy needs to be approximated as:

$$E_w \approx \sum_{i=1}^{N} P_w(t_i) \cdot \Delta t, \tag{16}$$

with $\Delta t = \frac{1}{f_{\text{sampling}}}$. Now an equivalent current profile is looked for, for which the difference is minimized between the energy calculated from the original profile and that from the equivalent profile. Specifically, the optimization aims to minimize the objective function:

$$G(X) = \sum_{i=1}^{N} \left(E_w - E_{eq}(X, t_i, v_i)\right)^2. \tag{17}$$

In this equation, $X = [t_{\text{rise}}, I_{\text{welding}}, t_{\text{welding}}, t_{\text{fall}}]$ represents the parameters of the equivalent current profile, which include the rise time, welding current, welding time, and fall time. These parameters and the shape of the equivalent current profile are illustrated in Figure 5.

Results The equivalent current profile is generated for each welded sample based on the measured signals. To test the effectiveness of this method, two finite element analyses are performed: one using the original current profile with 10,000 data points and one using the equivalent profile with 6 data points. Figure 6 illustrates the difference in the obtained weld diameter for the first five welded samples, demonstrating that the proposed method effectively preserves the weld diameter. When we compare those results using the percentage error as:

$$\epsilon_{\%} = \left| \frac{d_{\text{actual}} - d_{\text{equivalent}}}{d_{\text{actual}}} \right| \times 100 \tag{18}$$

we can see that this approach results in a substantial reduction in computation time, by a factor of 1.85 for a signal of 100,000 samples, with an average percentage error of only 0.894%. Moreover, it is evident that the error tends to be conservative, as the weld diameter is slightly underestimated, which favors safety.

3.2 Model validation

To assess the model's predictive capabilities, real-world measured data from the experiments are propagated through the FEM. This analysis focuses on predicting the variance in weld nugget diameters based on the input data variability. For all fifty welded samples, the generated equivalent current profiles are used as inputs for the finite element analysis. The electrode force was not measured and is considered constant at 2.5 kN in the FEA model. The simulated weld diameters are compared with the actual measured weld diameters, as illustrated in Figure 7a. It can be seen that the average predicted value of the weld diameters are similar. However, the FEM simulations show a narrower range of variability compared to the real-world measurements, suggesting that while the model captures the overall trend, it does not fully account for the variability observed in practice.

Variation on electrode force In the current method, only the variation in the current profile is considered, based on actual measured signals during welding. Although the electrode force was

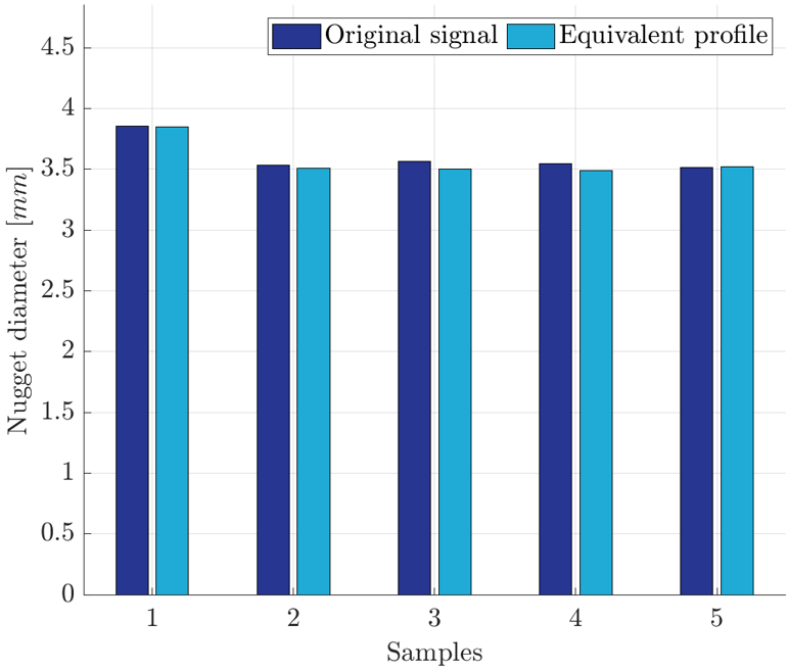

Figure 6: Comparison of nugget diameters of the original and equivalent current profile for 5 of the 50 samples

not measured, the sensitivity analysis of the model indicates that it also significantly influences weld formation. Future work will involve measuring the electrode force; for now, we assume that it varies in practice.

To estimate this potential variation of the electrode force, a deviation of 500 N from the nominal value of 2.5 kN is considered. This approach results in three simulations per welded sample: one at the nominal value and two at the extreme values of the electrode force. By plotting the resulting minimum and maximum simulated weld diameters as error bars, we obtain the graph shown in Figure 7b. Even if the variation in the electrode force falls within this range, it is still insufficient to replicate the full extent of variation observed in reality through simulations. Therefore, the variation observed is not solely attributable to the variability in input process (i.e., the current profile and electrode force).

4 CONCLUSIONS

The main goal of this work is to take initial steps to increase the industrial relevance of finite element models in spot welding applications. Incorporating uncertainty, which is inherent in an industrial environment, would be highly valuable in identifying robust welding parameters. These parameters—such as current, welding time, and contact pressure—should not only produce a sufficiently large weld diameter but also minimize variability with respect to the process input parameters. This study examines whether propagating the variation of the input process parameter, through the model results in a variation in weld diameter that aligns with the distribution observed in reality.

This paper presents a method to convert measured electrical current signals into a useful

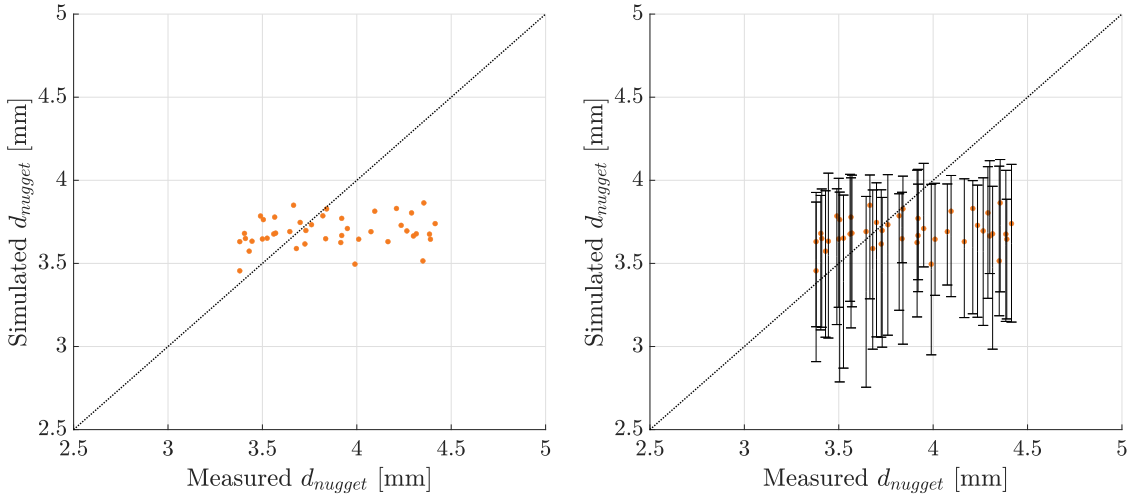

Figure 7: Comparison of nugget diameters between experiments and FEM simulations: (a) shows the comparison without considering the electrode force, while (b) includes the variation on the electrode force in the simulation.

equivalent to use as an input in finite element simulations, effectively addressing the computational challenges associated with processing large input time series. This method is based on conserving the energy input in the weld, while reducing the amount of data points to just 6 key data points. This approach ensures that the weld diameter is accurately predicted while significantly increasing computational efficiency. The effectiveness of this approach was validated through finite element analyses comparing the results obtained from the original 10.000-point current profile and the equivalent 6-point profile. The method results in a 65% reduction in computation time, with a rounded 1% error in the predicted value. Although this method was applied to an MFDC current signal, further research is needed to determine whether an equivalent current profile for AC or other types of current profiles can be converted in a similar manner.

After propagating the equivalent current profiles in the model, the distribution of the simulated weld diameters is compared with the distribution of the actually measured weld diameters. It becomes evident that the distribution of the measured nugget diameters is larger, indicating that the variation is not solely due to the electric current, despite its significant influence on weld formation. Furthermore, the sensitivity analysis reveals that the electrode force also has a major impact, and since it was not measured, it is incorporated as a vertex in the simulations. However, even with taking the electrode force into account, the resulting distribution still does not match the observed distribution in reality. This discrepancy underscores the need to consider modeling properties that cannot be directly measured, using lack-of-knowledge techniques to address these uncertainties. An inverse approach (as presented in [13]) could also be employed to estimate parameters such as contact resistances and the thickness of the contact layer.

ACKNOWLEDGEMENTS

The authors gratefully acknowledge the support of the Research Foundation – Flanders (FWO) under grant 1SE1423N and the internal funding of KU Leuven grant C24E/21/026.

REFERENCES

[1] A. O'Brien, *Welding Handbook, Vol. 3, Part 2: Welding Processes, 9th Edition*, vol. 3.

[2] Z. Wan, H. P. Wang, M. Wang, B. E. Carlson, and D. R. Sigler, "Numerical simulation of resistance spot welding of Al to zinc-coated steel with improved representation of contact interactions," *International Journal of Heat and Mass Transfer*, vol. 101, pp. 749–763, 2016.

[3] Y. B. Li, Z. Q. Lin, Q. Shen, and X. M. Lai, "Numerical analysis of transport phenomena in resistance spot welding process," *Journal of Manufacturing Science and Engineering, Transactions of the ASME*, vol. 133, no. 3, pp. 1–8, 2011.

[4] C. Böhne, G. Meschut, M. Biegler, J. Frei, and M. Rethmeier, "Prevention of liquid metal embrittlement cracks in resistance spot welds by adaption of electrode geometry," *Science and Technology of Welding and Joining*, vol. 25, no. 4, pp. 303–310, 2020.

[5] C. V. Nielsen, W. Zhang, L. M. Alves, N. Bay, and P. A. Martins, *Modeling of Thermo-Electro-Mechanical Manufacturing Processes with Applications in Metal Forming and Resistance Welding*. No. 9781447146421, 2013.

[6] T. Wanheim, N. Bay, and A. S. Petersen, "A theoretically determined model for friction in metal working processes," *Wear*, vol. 28, no. 2, pp. 251–258, 1974.

[7] M. Zwicker, N. Bay, and C. V. Nielsen, "A discussion of model asperities as a method to study friction in metal forming," *Discover Mechanical Engineering*, vol. 2, no. 1, 2023.

[8] M. Faes and D. Moens, *Recent Trends in the Modeling and Quantification of Non-probabilistic Uncertainty*, vol. 27. Springer Netherlands, 2020.

[9] A. Saltelli, M. Ratto, T. Andres, F. Campolongo, J. Cariboni, D. Gatelli, M. Saisana, and S. Tarantola, *Global Sensitivity Analysis. The Primer*, vol. 76. Wiley, dec 2007.

[10] I. M. Sobol', "Sensitivity Estimates for Nonlinear Mathematical Models," 1993.

[11] S. Marelli and B. Sudret, "UQLab: A Framework for Uncertainty Quantification in Matlab," in *Vulnerability, Uncertainty, and Risk*, (Reston, VA), pp. 2554–2563, American Society of Civil Engineers, jun 2014.

[12] A. Saltelli, S. Tarantola, F. Campolongo, and M. Ratto, *Sensitivity Analysis in Practice*. Wiley, feb 2002.

[13] M. Faes, M. Broggi, E. Patelli, Y. Govers, J. Mottershead, M. Beer, and D. Moens, "A multivariate interval approach for inverse uncertainty quantification with limited experimental data," *Mechanical Systems and Signal Processing*, vol. 118, no. November 2018, pp. 534–548, 2019.